IEEE Access
Multidisciplinary | Rapid Review | Open Access Journal

Received September 9, 2019, accepted September 25, 2019, date of publication September 27, 2019,
date of current version October 10, 2019.

Digital Object Identifier 10.1109/ACCESS.2019.2944257

Modelling of Implantable Drug Delivery System in Tumor Microenvironment Using Molecular Communication Paradigm

MUNEER M. AL-ZU'BI, (Student Member, IEEE), AND ANANDA SANAGAVARAPU MOHAN, (Senior Member, IEEE)

Centre for Health Technologies, Faculty of Engineering and Information Technology (FEIT), School of Biomedical Engineering, University of Technology Sydney, Ultimo, NSW 2007, Australia

Corresponding author: Ananda Sanagavarapu Mohan (ananda.sanagavarapu@uts.edu.au)

ABSTRACT Local delivery of anticancer drug in tumor using miniaturized implants over a prolonged period of time is a powerful treatment strategy that provides lower toxicity and higher drug bioavailability compared to conventional systemic chemotherapy. Prediction of anticancer drug distribution in tumor following implantation of the drug implant is necessary to improve and optimize the implantable drug delivery systems (IDDSs). In this paper, we develop mathematical and stochastic simulation models for the prediction of spatiotemporal concentration of anticancer doxorubicin following implantation of a dual-release implant in an isolated tumor microenvironment (TME). Our model utilizes mathematical convolution of the channel impulse response (CIR) with the drug release function based on the abstraction of molecular communication. The derived CIR can be used to obtain drug concentration profile in the surrounding tissue for various release profiles and different anticancer drugs. We derive closed-form analytical expression for anticancer drug concentration. The required release rates are obtained by fitting the experimental data on dual-release implant available in the literature to a mathematical expression. In addition, we also present a particle-based stochastic simulator and compare the results with those predicted by the analytical model. The accuracy of predictions by both the models is further verified by comparing with the published experimental data in the literature. Both the proposed models can be useful for the design optimization of the implantable drug delivery systems (IDDSs) in tumors and other tissues and can potentially reduce the number of animal experiments thus saving cost and time.

INDEX TERMS Cancer, concentration profile, drug delivery, doxorubicin, implant, molecular communication, stochastic simulation, tumor microenvironment.

I. INTRODUCTION

Cancer is a group of diseases characterized by uncontrolled growth and spread of abnormal cells [1]. Cancer can be treated using many treatment modalities, e.g., surgery, chemotherapy, etc. Although systemic drug delivery (conventional chemotherapy) is a preferred and widely used technique for anticancer drug administration, it suffers from poor drug bioavailability due to high elimination, enzymatic degradation, and other barriers as well as toxic side-effects due to accumulation in other healthy parts of the body [2]. Many alternative techniques of drug delivery for cancer treatment have already been introduced to overcome these limitations.

The associate editor coordinating the review of this manuscript and approving it for publication was Mohammad Upal Mahfuz.

Drug delivery from a miniaturized implant is one such technique which not only offers an efficient alternative but also can act as adjunctive therapy to other treatment techniques, particularly when the conventional therapies fail or can't be applied [3]. Also, the implantable drug delivery systems (IDDSs) have been found to offer lower toxicity and higher drug bioavailability compared to systemic chemotherapy [4]. In IDDS approach, the anticancer drug will be gradually delivered inside the tumor over a prolonged period of time, that may range from days to years without having to pass through the endothelial barrier of the tumor vasculature. In addition, the same implant could release a combination of different types of drugs. A polymeric membrane with controlled drug release was first proposed by Folkman and Long in 1964 who examined the use of silicone rubber

(Silastic®) for prolonged systemic drug administration [5]. Later, degradable polymer implants such as Gliadel® polymer and poly (lactic-co-glycolic acid) (PLGA) polymer have been clinically approved [6], [7].

Cancer cell death depends on the concentration of anticancer drug in its vicinity, where a minimum threshold level of drug concentration is required to destroy the cells. Drug concentration in tumor depends on the various biochemical and biophysical processes, such as drug release rate, diffusion properties of the environment, and drug elimination rate [8]. Knowledge of the spatiotemporal drug concentration profiles inside human tissues would be useful to design the IDDS and to minimize toxic levels at the healthy cells. Direct measurement of drug concentration in human tissues could be difficult and can't be readily obtained. Mathematical and stochastic models can be used to help understand and predict spatiotemporal drug distribution following insertion of drug implants in tumors. These models can be used together with both the animal experiments and clinical trials to improve the drug delivery system. Further, they may help to extend the in vivo results from animal models directly to humans thus offering a direct link between the laboratory experiments and clinical applications.

Most of the mathematical and simulation models for the transport and distribution of anticancer drugs in tumors are limited to systemic administration, i.e., via blood. A number of experimental studies have been reported on the measurement of drug concentration due to insertion of drug implants in tumors, e.g., [7], [9]–[21]. However, only a few studies on mathematical modelling of drug distribution due to tumor implants exist in the literature. A finite-difference numerical (computational) model for drug distribution and elimination in the vicinity of a polymer implant was developed in [22]. Analytical expressions for the prediction of the drug concentration of Carmustine (BiCNU®) in rat and monkey brain tissues were derived analytically in [23]–[25]. However, these models assume either a constant drug release pattern at the implant/tissue interface or use steady-state approximations. Numerical models for prediction of the transport parameters, e.g., diffusivity and elimination rate, following the release of doxorubicin (DOX) from dual-release polymer implant in liver tissues were proposed in [14], [19], [20]. In [26], [27], prediction of drug transport and clearance in the brain following drug release from polymers was obtained numerically using the finite-element method. The effect of various factors on the delivery of BCNU drug to brain tumors using polymers was examined using a computational finite-element model in [28]. A computational fluid dynamic model was developed for investigating the suitability of the transport of various chemotherapeutic drugs using polymeric wafers in brain tumor [29]. However, all these models use numerical methods to obtain solutions, thus lending themselves to many simplifying approximations that might reduce the accuracy of their prediction. Also, most of the reported models resort to unrealistic modelling of the release rate function; e.g., choosing either a constant or a simple decaying exponential function for the release rate. However, in most realistic drug implants, the drug release rate decreases with time after the insertion of the implant in the tissue. Thus, it is essential that the drug release models closely follow the release patterns revealed in the experimental investigations.

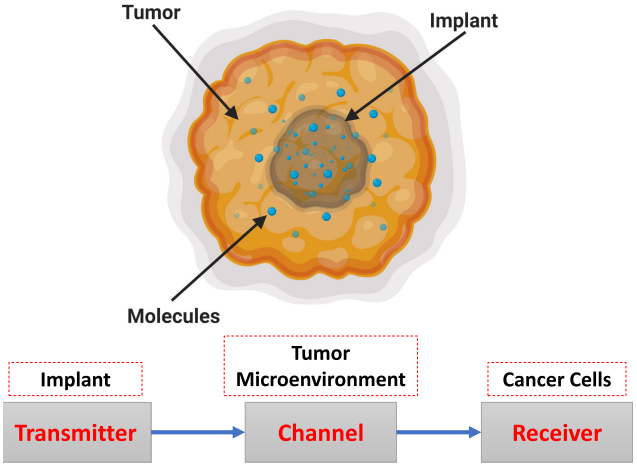

FIGURE 1. Molecular communication abstraction of implantable drug delivery system in a spherical tumor microenvironment. Created with BioRender.

In this paper, we propose novel analytical and stochastic simulation models for anticancer drug delivery into tumors using implantable drug delivery devices. Our models are aided by the abstraction offered by the molecular communication paradigm. The main contributions of this paper can be summarized as follows: (1) development of a new mathematical model for drug release and distribution of anticancer drug doxorubicin (DOX) following implantation of dual-release drug-loaded implant in the tumor using the molecular communication (MC) paradigm coupled with the convolution approach. The convolution approach is more general than the classical compartmental modeling approach [30]. The anticancer drug (DOX) is chosen because it is widely used in chemotherapy due to its efficacy in destroying a wide range of cancers [31]. In the MC paradigm, the implant is abstracted as a transmitter while the target site, i.e., malignant cell, is treated as a molecular receiver, as shown in Fig. 1. From the perspective of MC, DOX molecules represent the information molecules which are transported from the transmitter to the receiver. Here, the tumor microenvironment (TME) represents the propagation channel in which DOX molecules get randomly diffused from the transmitter to the receiver. (2) Another original contribution made in this paper is the modelling of the dynamics of drug release from the polymer implant as well as the distribution and elimination of drug molecules within the tumor tissue. (3) Development of convolution modelling by the derivation of a channel impulse response (CIR) to characterize the system components is another contribution of this paper. In contrast to other existing models, the analytical model proposed in this paper offers a more general approach for obtaining the spatiotemporal drug concentration profile to any drug release function of the

implant based on the convolution with the derived CIR in the time domain. (4) We employ realistic drug release rate function to develop a closed-form analytical expression for anticancer drug concentration profile in the tumor. This is done by fitting a mathematical function to the published experimental release data of dual-release implant [7]. (5) A stochastic random walk diffusion simulation model is also proposed for tracking the random Brownian motion of the molecules. The development of this stochastic model is completely independent of the proposed analytical model. Hence the stochastic model can be used to validate the analytical model. To the best of our knowledge, no stochastic simulation models have been reported so far for the release and distribution of anticancer drug in tumors using IDDSs.

The proposed analytical and stochastic models can help to predict the spatiotemporal drug concentration levels in the tumor and the surrounding healthy tissues, which helps to optimize the design of the IDDSs. Further, these models can also potentially contribute to reducing the number of experimental (or clinical) trials and thus will save time and cost. The proposed models can also be generalized to include drug transport in other tissues and even for delivering different drug molecules just by incorporating the tissue and drug-specific characteristic parameters.

The remainder of this paper is organized as follows. The mathematical derivation of the CIR and the release kinetic model are presented in section II. Also, the spatiotemporal drug concentration profile in the tumor is obtained by applying the convolution integral between the CIR and the release rate function. In section III, we describe the development of the stochastic particle-based simulator for DOX drug distribution in the vicinity of the implant and the surrounding tissue. Results obtained by both the analytical and stochastic simulation models are presented in section IV. These results are also compared with the experimental data extracted from the published literature [19]. Finally, a discussion is presented in section V, where the key contributions are highlighted.

II. DEVELOPMENT OF ANALYTICAL MODEL

In this section, we derive the spatiotemporal concentration profile in tumor tissues analytically. This is done by convolving the implant release function with the derived channel impulse response (CIR). Here, the drug source is assumed to be a miniaturized spherical implant located inside a spherically shaped isolated tumor, as shown schematically in Fig. 1. The implant is surrounded by biological tumor tissue, composed of cells and an extracellular space (ECS) filled with extracellular fluid (ECF). The implant is assumed to be loaded with anticancer drug doxorubicin (DOX) that is immediately released from the polymer into the vicinity of the implant after implantation. The released drug (DOX) will transport through the ECS (via diffusion and convection) and it may uptake by the cells through passive, active, or facilitated transport paths. Moreover, drugs could be eliminated into the systemic circulation via diffusion across the semipermeable membranes of capillaries. Also, drug molecules may be converted into other compounds due to various factors such as enzymes. Some molecules could bind to immobile elements in the surrounding tissue. All these processes could affect therapeutic efficacy.

Tumor tissues can be treated as porous media because the length scale of the intercapillary distances (i.e., the average distances between the capillaries) is much smaller than the length scale of the tumor radius [32]. Moreover, the tumor is assumed to be isolated from the surrounding healthy tissues [32]. We assume that the interstitial velocity field is very small and can be neglected throughout most parts of the tumor tissue. Therefore, drug transport in the interstitial space (porous medium) and drug elimination in tumor tissue are mathematically governed by the following diffusion equation:

$$\frac{\partial C}{\partial t} = D\nabla^2 C - \gamma C \tag{1}$$

where ∇^2 is Laplacian operator, C is the spatiotemporal distribution (concentration) of drug molecules in tumor tissue, D is the diffusion coefficient of the drug in tumor tissue in the unit of (m ^{2}/s), γ is the first-order elimination rate constant of drug due to various elimination processes, and t is the time after implantation.

When the binding/uptake process is much faster compared to the diffusion process, the local equilibrium between the free and bound molecules will be attained [33]. Therefore, the apparent diffusion coefficient (ADC) and the apparent first-order elimination rate constant can be expressed as follows, respectively, [20], [22]

$$D = \frac{D_w}{k_{bind} + 1} \tag{2}$$

$$\gamma = \frac{\gamma_w}{k_{bind} + 1} \tag{3}$$

where, D_w and γ_w is the drug diffusivity and lumped first-order elimination rate constant without including the binding effect. The parameter k_{bind} is the first-order binding constant of drug molecules with the target sites in the environment, e.g., cells, proteins, etc.

In the implantable drug delivery systems (IDDSs), the rapid elimination (perfusion) of drug molecules through capillaries is the most significant factor that affects the drug distribution. Assuming that the concentration of drug in the blood is small compared to that in the tissue and that the drug in the tissue is low enough for any enzymatic reactions, the elimination kinetics can be approximated to follow a first-order process [22], [26]. The elimination rate constant of the drug in the tumor can be defined as

$$\gamma_w = \gamma_v + \gamma_e + \gamma_o \tag{4}$$

where, γ_v is the drug loss rate constant due to perfusion through the capillaries (circulatory system), γ_e is the drug degradation rate constant due to the enzymatic reaction, and γ_o is the drug degradation rate constant due to other non-enzymatic factors. In this paper, we assume the drug loss

rate due to lymphatic drainage to be equal to zero, due to a lack of lymphatic system inside the tumors [13], [34]. The chemical alteration or degradation of drug molecules due to metabolism, such as enzymatic reaction, may convert drug molecules into other inactive substances.

A. CHANNEL IMPULSE RESPONSE

Assuming the tumor to be spherically shaped, Eq. (1) can be expressed in the spherically symmetric coordinate system, as

$$\frac{\partial \left(rC\left(r,t;r_0,t_0\right)\right)}{\partial t} = D\frac{\partial^2 \left(rC\left(r,t;r_0,t_0\right)\right)}{\partial r^2} - \gamma rC\left(r,t;r_0,t_0\right) \quad (5)$$

where $C\left(r,t;r_0,t_0\right)$ is the distribution of drug molecules at time t at radial position r from the center of the implant due to release of drug molecules at time t_0 at a radial position r_0. This distribution represents the final channel impulse response (CIR).

To obtain the CIR, the anticancer drug DOX is instantaneously released at the time $t = t_0$ at the spatial location $r = r_0$ from the implant. Thus, the following initial condition is applied:

$$C\left(r, t \to t_0\right) = \delta\left(r - r_0\right)\delta\left(t - t_0\right) \quad (6)$$

where r_0 is the implant radius and $\delta(\cdot)$ is Dirac Delta function.

In this model, two boundaries must be characterized, namely, the inner boundary at the center of the implant and the outer boundary at the tumor surface. Drug concentration is assumed to be finite at the center of the implant. This is applied via the following additional boundary condition:

$$C\left(r,t;r_0,t_0\right) \text{ is finite at } r \to 0 \quad (7)$$

Robin boundary condition [35], [36], is chosen as a general flux boundary condition at the outer surface of the tumor.

$$-D\nabla C\left(r,t;r_0,t_0\right)|_{r=r_t} = \omega\, C\left(r,t;r_0,t_0\right)|_{r=r_t} \quad (8)$$

where ω is the loss rate at the tumor boundary in the units of m/s. As a special case, by adjusting the loss rate ω, Robin boundary condition can be reduced either to a fully permeable (perfect-sink) case or an impermeable (no-flux) case.

The drug distribution at the location r and at the time t due to an instantaneous drug release from a point-like source at the position $r = r_0$ and at the time $t = t_0$ inside an unbounded medium can be written following [37], but only after the inclusion of a general initial releasing time and an elimination rate term as

$$C_u = \frac{1}{\left(4\pi D(t-t_0)\right)^{3/2}} \exp\left(-\frac{\|r-r_0\|^2}{4D(t-t_0)} - \gamma(t-t_0)\right) \quad (9)$$

where, $\|r - r_0\|$ is the separation distance between the drug point source and the observation point.

We assume that the drug molecules are uniformly distributed and released on the implant surface [44]–[46]. Thus, the drug distribution due to instantaneous drug release from the implant can be obtained by integrating Eq. (9) over the implant surface area (A_0) after transforming the parameters to the spherical coordinate system, as shown below:

$$C_s = \frac{1}{A_0} r_0^2 \int_0^{2\pi}\int_0^{\pi} C_u\left(r,\phi,\theta,t\right)\sin\left(\phi_0\right) d\phi_0 d\theta_0 \quad (10)$$

where $(0 \le \theta < 2\pi)$ is the azimuth angle and $(0 \le \phi \le \pi)$ is the polar angle.

By transforming Eq. (9) to a spherical coordinate system recognizing that the medium is spherically symmetric (i.e., $\phi = \theta = 0$), we get

$$C_u = \frac{1}{\left(4\pi D_t(t-t_0)\right)^{3/2}} \exp \times \left(-\frac{r_0^2 + r^2 - 2rr_0\cos(\phi_0)}{4D(t-t_0)} - \gamma(t-t_0)\right) \quad (11)$$

Substitution of Eq. (11) in (10) results in

$$C_s = \frac{1}{2\left(4\pi D(t-t_0)\right)^{3/2}} \exp\left(-\frac{r_0^2 + r^2}{4D(t-t_0)} - \gamma(t-t_0)\right) \times \int_0^{\pi} \exp\left(\frac{rr_0\cos(\phi_0)}{2D(t-t_0)}\right)\sin(\phi_0) d\phi_0 \quad (12)$$

Evaluating the integral in Eq. (12) using [38, eq. (3.915.1)], C_s can be written as

$$C_s = \frac{1}{4\pi r_0 r\left(4\pi D(t-t_0)\right)^{1/2}}\left[\exp\left(-\frac{(r-r_0)^2}{4D(t-t_0)} - \gamma(t-t_0)\right) - \exp\left(-\frac{(r+r_0)^2}{4D(t-t_0)} - \gamma(t-t_0)\right)\right] \quad (13)$$

Now apply the Laplace transform on Eq. (13) which can be evaluated with the help of [39, eq. (29.3.84)] to get

$$\tilde{C}_s = \frac{e^{\gamma t_0} e^{-st_0}}{4\pi r_0 rD\zeta} \times \begin{cases} e^{-r_0\zeta}\sinh\left(r\zeta\right), & r < r_0 \\ e^{-r\zeta}\sinh\left(r_0\zeta\right), & r > r_0 \end{cases} \quad (14)$$

where $\tilde{C}_s$ is the Laplace transform of C_s and

$$\zeta = \sqrt{(s+\gamma)/D} \quad (15)$$

The CIR due to an instantaneous (impulsive) drug release from the implant can be expressed as a superposition of two functions using a mathematical technique similar to that used in [40], [41],

$$C = C_s + C_b \quad (16)$$

Here, the parameters $(r, t; r_0, t_0)$ are omitted to simplify the mathematical notations. The total solution (16) can be written in the Laplace domain as

$$r\tilde{C} = r\tilde{C}_s + r\tilde{C}_b \quad (17)$$

where, $\tilde{C}$ is the Laplace transform of C and the multiplication factor r used to simplify the mathematical derivation.

The term C_b is the solution of the following diffusion equation which vanishes at $t = t_0$ and when it is added to C_s will satisfy the boundary conditions (7)–(8).

$$\frac{\partial (rC_b)}{\partial t} = D\frac{\partial^2 (rC_b)}{\partial r^2} - \gamma r C_b \tag{18}$$

Converting Eq. (18) into an ordinary differential equation (ODE) using Laplace transform to get

$$\frac{\partial^2 \left(r\tilde{C}_b\right)}{\partial r^2} - \zeta^2 r\tilde{C}_b = 0 \tag{19}$$

The diffusion equation (19) is a second-order ODE which has two roots at $\pm\zeta$. Thus, its solution can be expressed as

$$r\tilde{C}_b = A\sinh(r\zeta) + B\cosh(r\zeta) \tag{20}$$

After substituting Eqs. (14) and (20) in (17) for the case of $r > r_0$, we get

$$r\tilde{C} = \frac{e^{\gamma t_0} e^{-st_0} \sinh(r_0\zeta)\, e^{-r\zeta}}{4\pi r_0 D\zeta} H(r - r_0) + A\sinh(r\zeta) + B\cosh(r\zeta) \tag{21}$$

The general solution given by Eq. (21) should satisfy the boundary conditions (7)–(8) in the Laplace domain given by

$$\tilde{C} \text{ is finite at } r \to 0 \tag{22}$$

$$-D\left.\frac{\partial \tilde{C}}{\partial r}\right|_{r=r_t} = \omega\left.\tilde{C}\right|_{r=r_t} \tag{23}$$

We can rewrite the boundary condition (23) in an appropriate form to make the derivation mathematically tractable. Thus, using product rule of differentiation, we mathematically manipulate to get

$$\left.\frac{\partial \left(r\tilde{C}\right)}{\partial r}\right|_{r=r_t} = \left.\tilde{C}\right|_{r=r_t} + r_t\left.\frac{\partial \tilde{C}}{\partial r}\right|_{r=r_t} \tag{24}$$

Combining (23) and (24), we get

$$\left.\frac{\partial \left(r\tilde{C}\right)}{\partial r}\right|_{r=r_t} = r_t\lambda\left.\tilde{C}\right|_{r=r_t} \tag{25}$$

where,

$$\lambda = \frac{D - \omega r_t}{D r_t} \tag{26}$$

After applying the boundary conditions (22) and (25) to (21), we obtain the following expressions for A and B as

$$A = -\frac{e^{-st_0}}{4\pi r_0 D\zeta}\frac{e^{-r_t\zeta}\sinh(r_0\zeta)(\zeta + \lambda)}{(\lambda\sinh(r_t\zeta) - \zeta\cosh(r_t\zeta))} \tag{27}$$

$$B = 0 \tag{28}$$

The CIR is obtained by substituting (27)-(28) in (21) as

$$\tilde{C} = \frac{e^{-st_0}\sinh(r_0\zeta)}{4\pi r_0 rD\zeta\,(\lambda\sinh(r_t\zeta) - \zeta\cosh(r_t\zeta))} \times \left[e^{-r\zeta}(\lambda\sinh(r_t\zeta) - \zeta\cosh(r_t\zeta)) - e^{-r_t\zeta}\sinh(r\zeta)(\zeta + \lambda)\right] \tag{29}$$

The Inverse Laplace transform of (29) can be obtained using Cauchy's residue theorem [42],

$$C = \sum_{poles\ of\ \tilde{C}} \text{Res}\left(\tilde{C}e^{st}\right) \tag{30}$$

where Res($\tilde{C}$) is the residue of $\tilde{C}$.

The expression (29) has a simple pole at $s = -\gamma$ with zero residue and an infinite number of simple poles at $s = -(D\kappa_n^2/r_t^2 + \gamma)$ for n $= 1, 2, \ldots, \infty$. The parameter κ_n gives the real positive roots of the following equation:

$$\varphi(\kappa_n) = \lambda r_t \tan(\kappa_n) - \kappa_n \tag{31}$$

Thus, the Inverse Laplace transform of (29) can be written as

$$C = \frac{1}{2\pi r_0 r_t r}\sum_{n=1}^{\infty} e^{-(D\kappa_n^2/r_t^2+\gamma)(t-t_0)} e^{-i\kappa_n} \times \frac{\sin\left(r_0\kappa_n/r_t\right)\sin\left(r\kappa_n/r_t\right)(i\kappa_n + r_t\lambda)}{(\cos(\kappa_n)(\lambda r_t - 1) + \kappa_n\sin(\kappa_n))} \tag{32}$$

At the roots of Eq. (31), we get the following identity

$$\sin(\kappa_n) = \frac{\kappa_n}{\lambda r_t\cos(\kappa_n)} \tag{33}$$

Substituting (33) in (32) after applying Euler's formula on the complex exponentials ($e^{-i\kappa_n}$), we get

$$C = \frac{1}{2\pi r_0 r_t r}\sum_{n=1}^{\infty}\frac{\sin\left(\kappa_n r_0/r_t\right)\sin\left(\kappa_n r/r_t\right)}{\kappa_n^2 + \lambda r_t(\lambda r_t - 1)} \times \left(\kappa_n^2 + \lambda^2 r_t^2\right) e^{-(D\kappa_n^2/r_t^2+\gamma)(t-t_0)} \tag{34}$$

The equation (34) represents the CIR due to drug release instantaneously from a spherical drug implant following insertion inside an isolated spherical tumor. The equation (34) is an infinite series and has an infinite number of roots. However, this infinite series converges for a finite number of roots while the remaining roots have negligible effect and can be ignored. It must be recognized that the roots of $\varphi(\kappa_n)$ have a significant impact on the evaluation of Eq. (34). In order to evaluate (34) with higher accuracy, we have developed an accurate algorithm to find the roots of $\varphi(\kappa_n)$. The roots that have a negligible contribution to the final result have been discarded.

B. DRUG RELEASE KINETICS

The main design parameter for the implant is the release rate across the polymer surface. The release rates can be adjusted during the design phase by selecting appropriate materials and varying thickness of the polymer coating as well as the physicochemical variable properties of the loaded drug [43]. Moreover, the rate of drug release may also depend on the interactions between the drug and the tissue surrounding the implant as well as on the polymer-drug interaction, which in turn may affect the therapeutic process. In this release kinetic model, we assume that the implant releases DOX over two phases, viz., burst and sustained releases. During the burst release phase, the drug will be released with a fast

release rate over a short time followed by slow release over an extended period of time during the sustained release phase. For example, both the in-situ forming implants (ISFIs) [7], and the double-layer polymer implants [15] have dual release patterns. Thus, the cumulative amount of released DOX at time t can be mathematically modeled using the first-order bi-exponential kinetic model as

$$W(t) = W_\infty \left(1 - f_1 \cdot e^{-k_f t} - f_2 \cdot e^{-k_s t}\right) \quad (35)$$

where, $W(t)$ is the percentage of cumulative DOX released at time t, and W_∞ is the total percentage of DOX released at steady state. The parameters f_1 and f_2 are the DOX fractions released during the burst and sustained phases, respectively. The constants k_f and k_s are the release rate constants of burst and sustained release processes, respectively. We can also obtain a model only for the sustained release implant by just removing the burst release phase, i.e., $f_1 = 0$ in Eq. (35).

For an accurate representation of the release rate in the analysis, we use the bi-exponential kinetic model to fit the experimental release data of PLGA implants extracted from [7]. Using the nonlinear least-squares fitting method, we obtain the release rate constants as listed in Table 1. As shown in Fig. 2, the fitted curve shows good agreement with the experimental data with $R^2 = 0.9956$.

TABLE 1. Drug implant parameters.

Parameter	Value	Unit	Description
M_0	5	mg	Total loaded DOX in the implant. The implant can also be loaded with different amounts of the drug.
f_1	0.1	-	DOX fraction released during the burst phase [7].
f_2	0.9	-	DOX fraction released during the sustained phase (f_2=1-f_1) [7].
r_0	1	mm	Implant radius. The implant can have different sizes.
W_∞	88.9	%	Total percentage of DOX released at steady-state [7].
k_f	4.3×10^{-4}	s^{-1}	Burst release rate constant. It is obtained by fitting Eq. (35) to the experimental data in [7].
k_s	1.2×10^{-5}	s^{-1}	The sustained-release rate constant. It is obtained by fitting Eq. (35) to the experimental data in [7].

The cumulative amount of released DOX at time t can be expressed as

$$M(t) = M_0 W(t) \quad (36)$$

where M_0 is the total amount of loaded DOX in the implant in the unit of mg.

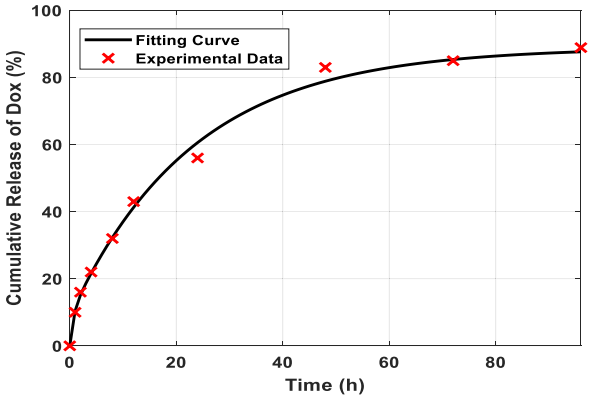

FIGURE 2. Percentage cumulative release of doxorubicin from the implant fitted to the published experimental data in [7], $R^2 = 0.9956$.

The drug release profile can be considered spatially uniform from the implant surface [44]–[46]. The drug release rate from the implant at time t can be expressed as

$$M_r(t) = \frac{dM}{dt} = M_0 W_\infty \left(k_f f_1 e^{-k_f t} + k_s f_2 e^{-k_s t}\right) \quad (37)$$

The drug release rate can be approximated as [24],

$$M_r(t) \approx \frac{M(t, t+\Delta t)}{\Delta t} = \frac{M(t+\Delta t) - M(t)}{\Delta t} \quad (38)$$

In this model, the size variation of the implant due to polymer biodegradation is assumed to be negligible during the observation time [7], [47].

C. DRUG CONCENTRATION PROFILE

Using the linear system analysis technique [30], drug concentration profile at any location inside the tumor can be obtained by applying the convolution between the CIR (34) and the release rate expression (37). After applying the convolution, we get the following spatiotemporal drug concentration profile,

$$\begin{aligned} P(r,t) &= \frac{M_0 W_\infty}{2\pi r_0 r_t r} \sum_{n=1}^{\infty} \frac{\sin\left(\kappa_n r_0/r_t\right) \sin\left(\kappa_n r/r_t\right)}{\kappa_n^2 + \lambda r_t\,(\lambda r_t - 1)} \\ &\times \left(\kappa_n^2 + \lambda^2 r_t^2\right) \int_{-\infty}^{\infty} e^{-\left(D\kappa_n^2/r_t^2 + \gamma\right)(\tau - t_0)} H(\tau - t_0) \\ &\times \left(k_f f_1 e^{-k_f(t-\tau)} + k_s f_2 e^{-k_s(t-\tau)}\right) H(t - \tau - t_0)\, d\tau \end{aligned} \quad (39)$$

where $H(t)$ is the unit (or Heaviside) step function.

By solving the integral in (39) assuming the initial release time t_0 is equal to zero, we get

$$\begin{aligned} P(r,t) = \frac{M_0 W_\infty}{2\pi r_0 r_t r} \sum_{n=1}^{\infty} \frac{\alpha_n \sin\left(\kappa_n r_0/r_t\right) \sin\left(\kappa_n r/r_t\right)}{\alpha_n - \lambda r_t} \\ \times \left(E_{fn} e^{-k_f t} + E_{sn} e^{-k_s t}\right) \end{aligned} \quad (40)$$

where,

$$E_{fn} = \frac{k_f f_1}{\beta_{fn}} \left(e^{\beta_{fn} t} - 1\right) \tag{41}$$

$$E_{sn} = \frac{k_s f_2}{\beta_{sn}} \left(e^{\beta_{sn} t} - 1\right) \tag{42}$$

$$\alpha_n = \kappa_n^2 + (\lambda r_t)^2 \tag{43}$$

$$\beta_{fn} = k_f - D\kappa_n^2 \Big/ r_t^2 - \gamma \tag{44}$$

$$\beta_{sn} = k_s - D\kappa_n^2 \Big/ r_t^2 - \gamma \tag{45}$$

III. STOCHASTIC SIMULATION MODEL

Stochastic simulations play an important role in understanding random diffusion and modelling of drug transport and interaction mechanisms. We implement a particle-based stochastic simulator in MATLAB for predicting drug release from a miniature spherical implant and for monitoring drug transport through the surrounding tissue in a spherically bounded 3-D tumor microenvironment. The total simulation time is divided into many small time-steps Δt.

The release process is performed according to experimentally fitted bi-exponential model following insertion of the implant inside the tumor. The amount of the released drug during each time-step, i.e., $[t, t + \Delta t]$, can be expressed as

$$M\,(t, t + \Delta t) = M\,(t + \Delta t) - M\,(t) \tag{46}$$

Substituting (35)-(36) in (46), we get

$$M\,(t, t + \Delta t) = M_0 W_\infty \left[f_1 \left(e^{-k_f t} - e^{-k_f (t+\Delta t)}\right) + f_2 \left(e^{-k_s t} - e^{-k_s (t+\Delta t)}\right)\right] \tag{47}$$

The number of released molecules can be expressed as $N_0 M(t, t + \Delta t) \big/ (M_0 W_\infty)$. However, to obtain the CIR using stochastic simulation, all the molecules must be released instantaneously, i.e., at the first-time step.

The movement of molecules in the extracellular matrix (ECM) of the tumor depends on the physiochemical properties of both the molecules and the ECM. The ECM is composed of networks of collagen fibers and other cells. Molecules diffuse through the spaces between network structures according to Brownian random walks. This random motion of molecules is influenced by the components of the ECM whose aggregate influence can be represented by using an apparent (or effective) diffusion coefficient (ADC). In the literature, it is common to use ADC to determine the diffusion of drugs in the ECM where ADC is equal to that in the real restricted extracellular matrix [48]. This allows us to use the ADC together with time-step to calculate the spatial displacements of molecules that follow random Brownian motion. Therefore, the released drug molecules will diffuse according to an independent random walk process (Brownian motion) in the simulation environment, i.e., tumor. The new position of each molecule is tracked and stored using the following equation [49]:

$$(x_i, y_i, z_i) = (x_{i-1}, y_{i-1}, z_{i-1}) + (\Delta x_i, \Delta y_i, \Delta z_i) \tag{48}$$

where, the index i refers to the current time-step, (x_i, y_i, z_i) are the coordinates of the current location of drug molecules at i^{th} time-step, $(x_{i-1}, y_{i-1}, z_{i-1})$ are the coordinates of the previous location of drug molecules at $(i\text{-}1)^{th}$ time-step, and $(\Delta x_i, \Delta y_i, \Delta z_i)$ is the random displacements which follow the normal distribution $N(0, \sigma^2)$ with zero mean and variance equal to $\sigma^2 = 2D\Delta t$.

The elimination of drug molecules in the simulation environment due to cellular uptake/binding, perfusion through blood vessels, and degradation are modelled using a first-order degradation reaction mechanism [22], [25]. At each time step, a uniformly distributed random number R_1 between zero and one is generated for each molecule. Then, the generated random numbers are compared with the elimination probability in Eq. (49) [50]:

$$P_\gamma = 1 - \exp(-\gamma \Delta t) \tag{49}$$

If the elimination probability is larger than the random number R_1, the molecule will be removed from the simulation environment.

The outer surface of the simulation environment (tumor) is modelled as a general partially reflecting boundary, which is mathematically equivalent to the Robin boundary condition used in our analytical model given in section II. Some of the molecules will be reflected when they reach the boundary and others will be removed from the environment. This condition can represent the effect of DOX elimination to the neighboring tissue or leakage into the exchange blood and lymphatic vessels at the outer boundary of the tumor where many exchange vessels exist that may act as sinks for drug molecules [32]. The partially reflecting boundary condition can be reduced to other special cases, e.g., no-flux (fully reflecting) boundary.

A uniformly distributed random number R_2, between zero and one, is assigned to each molecule that hits the medium boundary. Then, if the forward reaction probability, given by Eq. (50), is larger than the random number R_2, the drug molecule will be removed from the simulation environment [41]:

$$P_\omega = \omega \sqrt{\frac{\pi \Delta t}{D}} \tag{50}$$

Otherwise, the drug molecule will reflect back to the previous location inside the environment.

The impermeable (no-flux) boundary condition can be used when no molecule transmission takes place at the boundary, i.e., $\omega = 0$. On the other hand, when each collision between molecule and boundary leads to transmission, a fully permeable boundary condition can be applied, i.e., $\omega \to \infty$. The interaction of drug molecules with the medium boundary occurs within a short period of time. Therefore, the time step should be small enough for modelling the interaction and permeation of drug molecules at the medium boundary.

The spatiotemporal drug concentration profile inside the simulation environment can be estimated using a virtual spherical observer that does not hinder movements of

the molecules. At each time step, the drug molecules that enter the observer volume will contribute to the total received molecules. Then, the drug concentration profile can be obtained as follows

$$P_{sim}(r,t) = M_0 W_\infty \frac{N}{N_0 V_{rx}} \tag{51}$$

where N is the total number of the received molecules, N_0 is the total number of released molecules from the implant, and V_{rx} is the receiver (or observer) volume.

IV. RESULTS

In this section, we will first examine the accuracy of the CIR, given in (34), which is the basis for deriving the drug concentration profile. Then, we examine the effect of various system parameters on the transport of anticancer drug DOX in terms of the drug concentration profile and the maximum concentration after implantation of the dual-release implant in the tumor. The results are obtained using both the proposed models, viz., analytical model and stochastic particle-based simulator. Also, accuracy of the predicted results by our proposed models is verified by comparing with the published experimental data on DOX bio-distribution in tumor extracted from [19]. The system parameters used in our computations are listed in Tables 1 and 2.

TABLE 2. System parameters (unless stated otherwise).

Parameter	Value	Unit
T	150	h
Δt	0.1	h
N_0	10^5	molecule
D	4×10^{-11}	m^2/s
ω	10	µm/s
γ	5×10^{-6}	s^{-1}
r_t	10	mm
r_{rx}	0.5	mm
r	5	mm
Iterations	100	-

The diffusivity of DOX inside the tumor is chosen to fall within the range of the experimentally measured data published in [14], [51]. To choose optimal values for the simulation parameters, we first conduct a trial and error run with different values of the time-step and the number of transmitted molecules to examine the concentration profile variations. For example, when the time-step is less than 0.1h, we found no significant change and variation in the simulation results. We chose the tumor radius in our models to be equal to 1 cm. This value falls within the range of different tumor sizes encountered in reality, e.g., the diameter of tumors in rat and rabbit ranges from 0.5 to 2 cm [52]. The radius of the virtual observer (r_{rx}) is chosen to be 0.5 mm so that enough molecules can contribute to estimating the concentration within the receiver volume. The elimination rate constant (γ) also has a range of values, and thus different values are chosen for the calculations to examine its effect on the drug distribution profile [14].

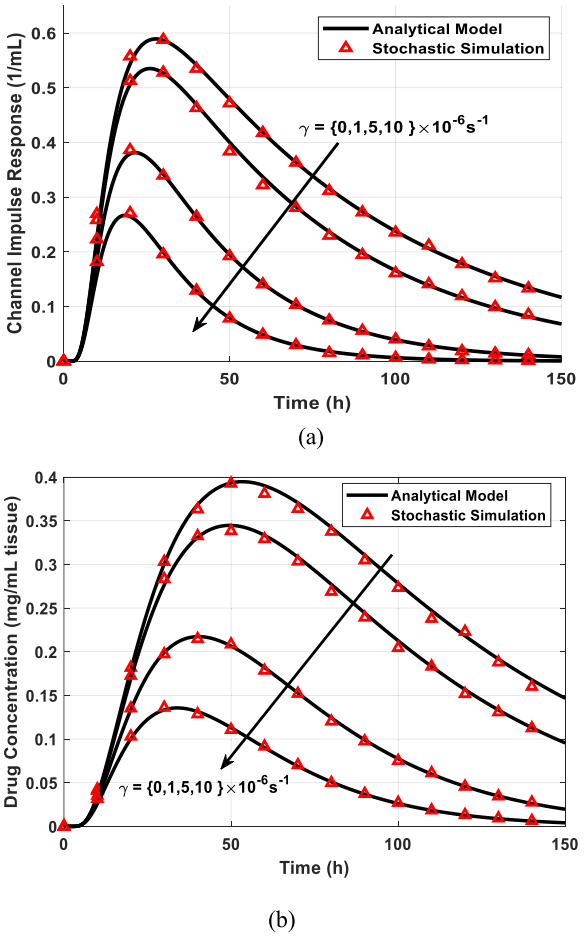

FIGURE 3. (a) Channel impulse response and (b) drug concentration profile for various values of drug elimination (loss) rate in the tumor.

In Fig. 3, we plot the CIR and the drug concentration profile for different values of the elimination rates. The results in this figure indicate a similar trend. The analytical results obtained using the expressions (34) and (40), match well with the stochastic simulation results. Thus, the agreement of the results obtained from the two independent models demonstrates the validation of the modelling approaches proposed in this paper. As expected, an increase in the elimination rate due to different factors, e.g., vascular perfusion, cellular uptake, enzymatic and non-enzymatic metabolisms, etc., will result in a decrease of the drug concentration in the tumor. The drug metabolisms and drug clearance through the capillaries reduce the amount of the drug in the tissue. Therefore, fast metabolic rate leads to higher biotransformation of drug in the tissue compared to low metabolic rate Moreover, drug concentration increases with the time until reaching the peak concentration and then it decreases gradually to a minimal value.

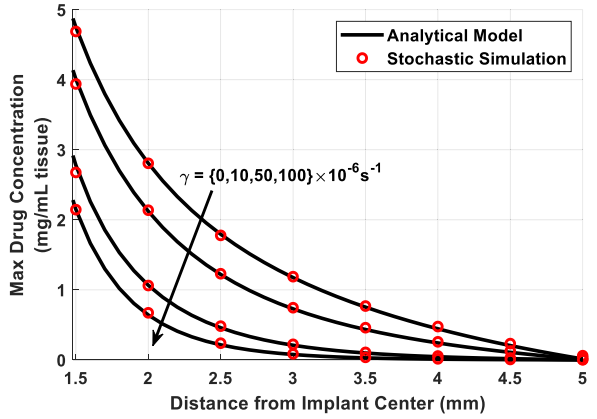

FIGURE 4. Maximum drug concentration versus distance from the implant center for different elimination rate constants when $\omega = 1\mu$m/s and $r_t = 5$mm.

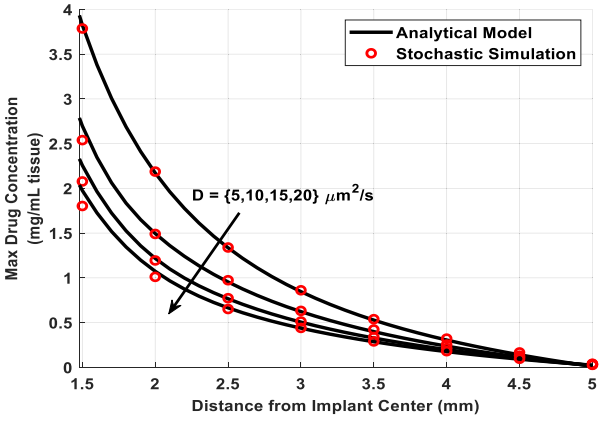

FIGURE 5. Maximum drug concentration versus distance from the implant center for various diffusion coefficients when $\omega = 1\mu$m/s and $r_t = 5$mm.

The maximum (or peak) drug concentration C_{max} and the corresponding peak time t_{max} at a specified location in the tissue represent important pharmacokinetic metrics. In this section, these metrics are obtained from the drug concentration profile using the analytical and simulation models presented in the previous sections. Figures 4 and 5 show the maximum drug concentration as a function of the separation distance from the implant center For the simulation model, since the radius of the virtual observer $r_{rx} = 0.5$ mm, we need to start recording the concentration at a distance 0.5mm from the implant surface (i.e., 1.5 mm from the centre of the implant) to avoid intersection of the virtual observer (receiver) with the implant. The results in this figure are obtained using both the proposed models for various drug elimination rates. Drug concentration decreases as the distance from the implant increases and finally reach zero at the tumor boundary. Moreover, the higher elimination rate will lead to lower maximum drug concentration as shown in Fig. 4. Also, the effective drug diffusivity has an impact on transport and distribution of drug in the tumor, as shown in Fig. 5, where the higher diffusivity leads to lower peak concentration.

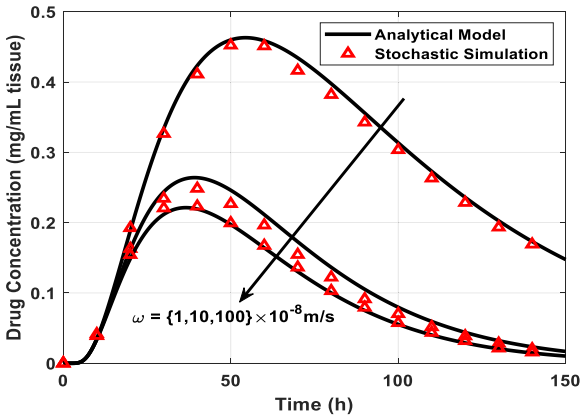

FIGURE 6. Drug concentration profile as a function of time for different loss rates at the tumor boundary.

Figure 6 shows the impact of the loss rate at the tumor boundary on the drug concentration profile inside the tumor tissue. Drug concentration decreases as the loss rate increases. This happens because the probability of drug elimination through the boundary will increase with the increase in the loss rate. Adding the loss rate ω to our model via Robin boundary condition allows us to select the appropriate boundary condition at the tumor boundary by adjusting the value of ω, e.g., $\omega = 0$ leads to no-flux at the boundary.

Impact of the sustained release rate on both the maximum drug concentration and the corresponding time instant is plotted versus the separation distance from the implant center in Fig. 7. As shown in Fig. 7a, the maximum drug concertation increases as the sustained release rate increases because more drug will be released from the implant within a shorter time. Impact of the sustained release rate on the maximum drug concentration decreases as the distance from the implant increases and finally the maximum concentration converges for all the release rates because the distance becomes the main dominant factor. On the other hand, the time at which the concentration is maximum becomes shorter with the increase in sustained release rate as shown in Fig. 7b, since a higher amount of drug will be released within a shorter time.

To verify the accuracy and validity of our proposed models we compare the results predicted by both of our proposed models with the published experimental data extracted from [19]. The experimental data provides measured DOX concentration with the distance from polymer implant placed in a liver tumor. Drug transport from this implant to the surrounding tissue is symmetric around the implant axis due to the geometry of the implant. To compare the results from our models with the measured data on DOX distribution, we use the same diameter of the implant and the tumor as that used in [19], i.e., 1.6 mm and 1.1cm, respectively. We estimate the implant release rate constant (0.5341 day^{-1}) by curve fitting the releasing rate characteristics given in [19]. The amount of loaded DOX in the implant is 2.99 mg and 93.7% of the loaded drug is released on the fourth day,

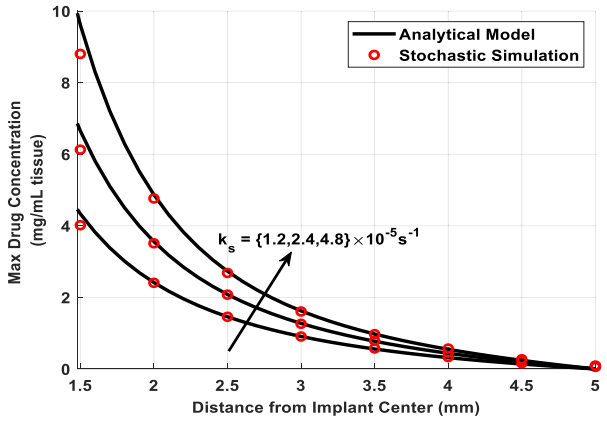

(a)

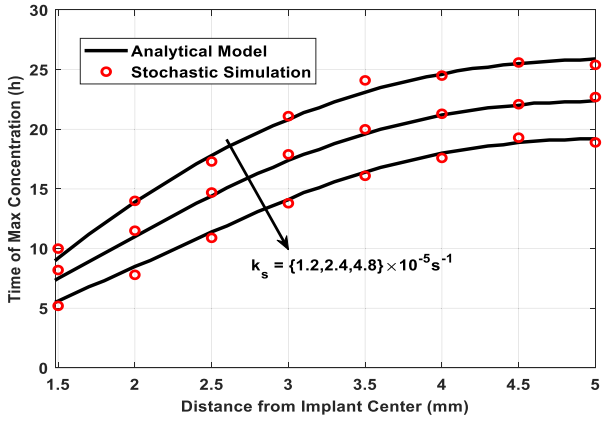

(b)

FIGURE 7. (a) Maximum drug concentration and (b) peak time versus distance from the implant center for various sustained release rate constants.

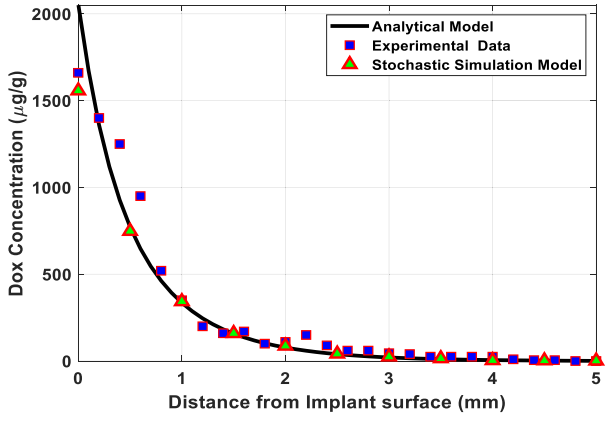

FIGURE 8. Drug concentration (on the fourth day) versus the distance from the implant/tumor interface compared to the mean value of published experimental data taken from [19].

i.e., 2.8 mg. These data are extracted from the experimental data given in literature and are used to compute our results [16], [19].

The apparent diffusivity and apparent elimination rate constant of DOX in liver tumor tissue are given as $D = 50\ \mu m^2/s$ and $\gamma = 0.58 \times 10^{-4}\ s^{-1}$ respectively [14]. The density of tumor and liver tissues is equal to $\sim 1.04\ g/cm^3$; therefore volume can be replaced with mass for obtaining the concentration in unit of (μg/g) [53], [54].

Figure 8 shows a comparison of DOX concentration obtained using our proposed models with the published experimental data as a function of the radial distance from the implant surface on the fourth day after implantation in the tumor. It can be seen that the results obtained using our analytical and stochastic models agree well with the results extracted from the published experimental data in [19]. As expected, the measured concentration shows a decreasing trend with the radial distance from the implant. In general, our proposed models can predict the DOX concentration in the tumor at different radial distances from the implant accurately. Moreover, the experimental data extracted from the literature and plotted in this figure represent the mean values, and the predicted results by our models fall within the standard deviation of the mean.

V. CONCLUSION

In this paper, we have proposed analytical and stochastic simulation models based on molecular communication paradigm for predicting the release and distribution of anticancer drug doxorubicin (DOX) in an isolated tumor following implantation of a dual-release implant. We derive a closed-form analytical expression of DOX concentration profile in the tumor by applying the convolution between the implant release function and the derived channel impulse response (CIR). In addition, we develop a stochastic simulation approach to model the DOX drug release from the implant and for monitoring the distribution of drug molecules in the surrounding tumour tissue. Accuracy and validity of the proposed models can be seen from the comparison with the experimental data given in the literature. Impact of the various parameters on the drug concentration profile and the CIR, i.e., elimination rate, diffusivity, loss rate at the tumor boundary, and the implant release rates, are examined. Also, the analytical and simulation results of the peak time and drug peak concentration are obtained with respect to the radial distance from the centre of the implant. The proposed models can help to optimize the design and deployment of the implantable drug delivery systems (IDDSs) in tumors or any other tissues by adjusting the system parameters. Although we derive the drug concentration profile for the first-order bi-exponential kinetic model, the CIR can be used for modelling other implants that may have different drug release patterns.

REFERENCES

[1] *Cancer Facts & Figures*, Amer. Cancer Soc., Atlanta, GA, USA, 2019.
[2] Y. H. Bae and K. Park, "Targeted drug delivery to tumors: Myths, reality and possibility," *J. Controlled Release*, vol. 153, pp. 198–205, Aug. 2011.
[3] J. B. Wolinsky, Y. L. Colson, and M. W. Grinstaff, "Local drug delivery strategies for cancer treatment: Gels, nanoparticles, polymeric films, rods, and wafers," *J. Controlled Release*, vol. 159, no. 1, pp. 14–26, Apr. 2012.
[4] D. Rosenblum, N. Joshi, W. Tao, J. M. Karp, and D. Peer, "Progress and challenges towards targeted delivery of cancer therapeutics," *Nature Commun.*, vol. 9, no. 1, Apr. 2018, Art. no. 1410.

[5] J. Folkman and D. M. Long, "The use of silicone rubber as a carrier for prolonged drug therapy," *J. Surg. Res.*, vol. 4, no. 3, pp. 139–142, 1964.

[6] A. J. Sawyer, J. K. Saucier-Sawyer, C. J. Booth, J. Liu, T. Patel, J. M. Piepmeier, and W. M. Saltzman, "Convection-enhanced delivery of camptothecin-loaded polymer nanoparticles for treatment of intracranial tumors," *Drug Del. Transl. Res.*, vol. 1, no. 1, pp. 34–42, Feb. 2011.

[7] J. Li, T. Krupka, J. Yao, R. Wang, L. Jiang, Y. Zhou, G. Zuo, Z. Wang, L. Dai, J. Ren, and Y. Zheng, "Liquid-solid phase-inversion PLGA implant for the treatment of residual tumor tissue after HIFU ablation," *PLoS ONE*, vol. 10, no. 2, 2015, Art. no. e0117358.

[8] M. Kim, R. J. Gillies, and K. A. Rejniak, "Current advances in mathematical modeling of anti-cancer drug penetration into tumor tissues," *J. Frontiers Oncol.*, vol. 3, p. 278, Nov. 2013.

[9] L. Gao, L. Xia, R. Zhang, D. Duan, X. Liu, J. Xu, and L. Luo, "Enhanced antitumor efficacy of poly(D,L-lactide-co-glycolide)-based methotrexate-loaded implants on sarcoma 180 tumor-bearing mice," *Drug Des. Develop. Therapy*, vol. 11, pp. 3065–3075, Oct. 2017.

[10] U. Edlund and A.-C. Albertsson, "Degradable polymer microspheres for controlled drug delivery," in *Degradable Aliphatic Polyesters*. Berlin, Germany: Springer, 2002, pp. 67–112.

[11] V. R. Sinha and A. Trehan, "Biodegradable microspheres for protein delivery," *J. Controlled Release*, vol. 90, no. 3, pp. 261–280, Jul. 2003.

[12] S. Freiberg and X. X. Zhu, "Polymer microspheres for controlled drug release," *Int. J. Pharmaceutics*, vol. 282, nos. 1–2, pp. 1–18, Sep. 2004.

[13] A. Shemi, E. Z. Khvalevsky, R. M. Gabai, A. Domb, and Y. Barenholz, "Multistep, effective drug distribution within solid tumors," *Oncotarget*, vol. 6, no. 37, 2015, Art. no. 39564.

[14] B. D. Weinberg, R. B. Patel, A. A. Exner, G. M. Saidel, and J. Gao, "Modeling doxorubicin transport to improve intratumoral drug delivery to RF ablated tumors," *J. Controlled Release*, vol. 124, nos. 1–2, pp. 9–11, Dec. 2007.

[15] F. Qian, G. M. Saidel, D. M. Sutton, A. Exner, and J. Gao, "Combined modeling and experimental approach for the development of dual-release polymer millirods," *J. Controlled Release*, vol. 83, no. 3, pp. 427–435, 2002.

[16] B. D. Weinberg, E. Blanco, S. F. Lempka, J. M. Anderson, A. A. Exner, and J. Gao, "Combined radiofrequency ablation and doxorubicin-eluting polymer implants for liver cancer treatment," *J. Biomed. Mater. Res. A*, vol. 81, no. 1, pp. 205–213, Apr. 2007.

[17] J. R. Haaga, A. A. Exner, Y. Wang, N. T. Stowe, and P. J. Tarcha, "Combined tumor therapy by using radiofrequency ablation and 5-FU–Laden polymer implants: Evaluation in rats and rabbits," *Radiology*, vol. 237, no. 3, pp. 911–918, 2005.

[18] J. Gao, F. Qian, A. Szymanski-Exner, N. Stowe, and J. Haaga, "*In vivo* drug distribution dynamics in thermoablated and normal rabbit livers from biodegradable polymers," *J. Biomed. Mater. Res.*, vol. 62, no. 2, pp. 308–314, Nov. 2002.

[19] B. D. Weinberg, E. Blanco, and J. Gao, "Polymer implants for intratumoral drug delivery and cancer therapy," *J. Pharmaceutical Sci.*, vol. 97, no. 5, pp. 1681–1702, May 2008.

[20] F. Qian, N. Stowe, E. H. Liu, G. M. Saidel, and J. Gao, "Quantification of *in vivo* doxorubicin transport from PLGA millirods in thermoablated rat livers," *J. Controlled Release*, vol. 91, nos. 1–2, pp. 157–166, Aug. 2003.

[21] A. W. Wong, B. Z. Fite, Y. Liu, A. Kheirolomoom, J. W. Seo, K. D. Watson, L. M. Mahakian, S. M. Tam, H. Zhang, J. Foiret, A. D. Borowsky, and K. W. Ferrara, "Ultrasound ablation enhances drug accumulation and survival in mammary carcinoma models," *J. Clin. Invest.*, vol. 126, no. 1, pp. 99–111, 2016.

[22] W. M. Saltzman and M. L. Radomsky, "Drugs released from polymers: Diffusion and elimination in brain tissue," *Chem. Eng. Sci.*, vol. 46, no. 10, pp. 2429–2444, 1991.

[23] L. K. Fung, M. Shin, B. Tyler, H. Brem, and W. M. Saltzman, "Chemotherapeutic drugs released from polymers: Distribution of 1,3-bis(2-chloroethyl)-l-nitrosourea in the rat brain," *Pharmaceutical Res.*, vol. 13, no. 5, pp. 671–682, 1996.

[24] L. K. Fung, M. G. Ewend, A. Sills, E. P. Sipos, R. Thompson, M. Watts, O. M. Colvin, H. Brem, and W. M. Saltzman, "Pharmacokinetics of interstitial delivery of carmustine, 4-hydroperoxycyclophosphamide, and paclitaxel from a biodegradable polymer implant in the monkey brain," *Cancer Res.*, vol. 58, no. 4, pp. 672–684, Feb. 1998.

[25] J. F. Strasser, L. K. Fung, S. Eller, S. A. Grossman, and W. M. Saltzman, "Distribution of 1,3-bis(2-chloroethyl)-1-nitrosourea and tracers in the rabbit brain after interstitial delivery by biodegradable polymer implants," *J. Pharmacol. Exp. Therapeutics*, vol. 275, no. 3, pp. 1647–1655, Dec. 1995.

[26] B. Reisfeld, S. Kalyanasundaram, and K. Leong, "A mathematical model of polymeric controlled drug release and transport in the brain," *J. Controlled Release*, vol. 36, no. 3, pp. 199–207, 1995.

[27] S. Kalyanasundaram, V. D. Calhoun, and K. W. Leong, "A finite element model for predicting the distribution of drugs delivered intracranially to the brain," *Amer. J. Physiol.*, vol. 273, no. 5, pp. R1810–R1821, Nov. 1997.

[28] C. C. Wang, J. Li, C. S. Teo, and T. Lee, "The delivery of BCNU to brain tumors," *J. Controlled Release*, vol. 61, nos. 1–2, pp. 21–41, Aug. 1999.

[29] D. Y. Arifin, K. Y. Lee, and C. H. Wang, "Chemotherapeutic drug transport to brain tumor," *J. Controlled Release*, vol. 137, no. 3, pp. 203–210, Aug. 2009.

[30] L. Rosso, C. S. Brock, J. M. Gallo, A. Saleem, P. M. Price, F. E. Turkheimer, and E. O. Aboagye, "A new model for prediction of drug distribution in tumor and normal tissues: Pharmacokinetics of temozolomide in glioma patients," *Cancer Res.*, vol. 69, no. 1, pp. 120–127, Jan. 2009.

[31] C. Carvalho, R. X. Santos, S. Cardoso, S. Correia, P. J. Oliveira, M. S. Santos, and P. I. Moreira, "Doxorubicin: The good, the bad and the ugly effect," *Current Med. Chem.*, vol. 16, no. 25, pp. 3267–3285, 2009.

[32] M. Soltani and P. Chen, "Numerical modeling of fluid flow in solid tumors," *PLoS ONE*, vol. 6, no. 6, 2011, Art. no. e20344.

[33] C. Nicholson, "Diffusion and related transport mechanisms in brain tissue," *Rep. Progr. Phys.*, vol. 64, no. 7, p. 815, 2001.

[34] W. Zhan and X. Y. Xu, "A mathematical model for thermosensitive liposomal delivery of doxorubicin to solid tumour," *J. Drug Del.*, vol. 2013, Dec. 2013, Art. no. 172529.

[35] K. Gustafson and T. Abe, "The third boundary condition—Was it Robin's?" *Math. Intell.*, vol. 20, no. 1, pp. 63–71, 1998.

[36] S. S. Andrews, "Accurate particle-based simulation of adsorption, desorption and partial transmission," *Phys. Biol.*, vol. 6, no. 4, p. 046015, Nov. 2009.

[37] I. Llatser, A. Cabellos-Aparicio, M. Pierobon, and E. Alarcon, "Detection techniques for diffusion-based molecular communication," *IEEE J. Sel. Areas Commun.*, vol. 31, no. 12, pp. 726–734, Dec. 2013.

[38] A. Jeffrey and D. Zwillinger, *Table of Integrals, Series, and Products*. Amsterdam, The Netherlands: Elsevier, 2007.

[39] M. Abramowitz and I. A. Stegun, *Handbook of Mathematical Functions: With Formulas, Graphs, and Mathematical Tables*. New York, NY, USA: Dover, 1964.

[40] K. Schulten and I. Kosztin, *Lectures in Theoretical Biophysics*, vol. 117. Champaign, IL, USA: Univ. Illinois, 2000.

[41] Y. Deng, A. Noel, M. Elkashlan, A. Nallanathan, and K. C. Cheung, "Modeling and simulation of molecular communication systems with a reversible adsorption receiver," *IEEE Trans. Mol. Biol. Multi-Scale Commun.*, vol. 1, no. 4, pp. 347–362, Dec. 2015.

[42] R. P. Agarwal, K. Perera, and S. Pinelas, *An Introduction to Complex Analysis*. New York, NY, USA: Springer, 2011.

[43] W. W. Yang and E. Pierstorff, "Reservoir-based polymer drug delivery systems," *J. Lab. Autom.*, vol. 17, no. 1, pp. 50–58, Feb. 2012.

[44] A. F. C. Resende, A. F. Pereira, T. P. Moreira, P. S. O. Patrício, S. L. Fialho, G. M. F. Cunha, A. Silva-Cunha, J. T. Magalhães, and G. R. Silva, "PLGA Implants containing vancomycin and dexamethasone: Development, characterization and bactericidal effects," *Die Pharmazie-Int. J. Pharmaceutical Sci.*, vol. 71, no. 8, pp. 439–446, 2016.

[45] K. Wang, X. Zhang, L. Zhang, L. Qian, C. Liu, J. Zheng, and Y. Jiang, "Development of biodegradable polymeric implants of RGD-modified PEG-PAMAM-DOX conjugates for long-term intratumoral release," *Drug Del.*, vol. 22, no. 3, pp. 389–399, May 2015.

[46] L. Tamaddon, S. A. Mostafavi, R. Karkhane, M. Riazi-Esfahani, F. A. Dorkoosh, and M. Rafiee-Tehrani, "Design and development of intraocular polymeric implant systems for long-term controlled-release of clindamycin phosphate for toxoplasmic retinochoroiditis," *Adv. Biomed. Res.*, vol. 4, p. 32, Jan. 2015.

[47] D. Y. Pereira, A. T. Yip, B. S. Lee, and D. T. Kamei, "Modeling mass transfer from carmustine-loaded polymeric implants for malignant gliomas," *J. Lab. Autom.*, vol. 19, no. 1, pp. 19–34, Feb. 2014.

[48] E. Syková and C. Nicholson, "Diffusion in brain extracellular space," *Physiol. Rev.*, vol. 88, no. 4, pp. 1277–1340, Oct. 2008.

[49] Y. Lu, M. D. Higgins, A. Noel, M. S. Leeson, and Y. Chen, "The effect of two receivers on broadcast molecular communication systems," *IEEE Trans. Nanobiosci.*, vol. 15, no. 8, pp. 891–900, Dec. 2016.
[50] A. Ahmadzadeh, H. Arjmandi, A. Burkovski, and R. Schober, "Comprehensive reactive receiver modeling for diffusive molecular communication systems: Reversible binding, molecule degradation, and finite number of receptors," *IEEE Trans. Nanobiosci.*, vol. 15, no. 7, pp. 713–727, Oct. 2016.
[51] B. J. Toley, Z. G. T. Lovatt, J. L. Harrington, and N. S. Forbes, "Microfluidic technique to measure intratumoral transport and calculate drug efficacy shows that binding is essential for doxorubicin and release hampers Doxil," *Integr. Biol.*, vol. 5, no. 9, pp. 1184–1196, 2013.
[52] M. A. Burton, B. N. Gray, G. W. Self, J. C. Heggie, and P. S. Townsend, "Manipulation of experimental rat and rabbit liver tumor blood flow with angiotensin II," *Cancer Res.*, vol. 45, no. 11, pp. 5390–5393, 1985.
[53] S. A. Gulec, G. Mesoloras, and M. Stabin, "Dosimetric techniques in 90Y-microsphere therapy of liver cancer: The MIRD equations for dose calculations," *J. Nucl. Med.*, vol. 47, no. 7, pp. 1209–1211, 2006.
[54] M. Montelius, M. Ljungberg, M. Horn, and E. Forssell-Aronsson, "Tumour size measurement in a mouse model using high resolution MRI," *BMC Med. Imag.*, vol. 12, no. 1, p. 12, 2012.

MUNEER M. AL-ZU'BI received the B.Sc. degree (Hons.) in communication and software engineering from Al-Balqa Applied University, Jordan, in 2010, and the M.Sc. degree (Hons.) in wireless communications from the Jordan University of Science and Technology (JUST), Jordan, in 2014. He is currently pursuing the Ph.D. degree with the School of Biomedical Engineering, University of Technology Sydney (UTS). He was a Research Assistant with JUST and a Communication Engineer with the King Abdullah II Design and Development Bureau (KADDB), Jordan, before joining UTS, in 2016. He was a recipient of the many scholarships during his studies. He designed many innovative hardware and software projects in the areas of telecommunication, computer, and biomedical engineering. His main research interests include molecular communications, wireless communications for biomedical applications, bio-nanomachines, and EM wave propagation.

ANANDA SANAGAVARAPU MOHAN (A. S. MOHAN) (SM'05) received the Ph.D. degree from the Indian Institute of Technology Kharagpur, India. He was formerly the Co-Director of the Microwave Design Centre with UTS, and also an Associate Director of the UTS node of the Multi University Co-operative Research Centre on Satellite Systems. Before joining UTS, he held a postdoctoral fellowship position with the Air Navigation Research Group, School of Electrical Engineering, The University of Sydney, Australia. He is currently an Associate Professor with the Faculty of Engineering and Information Technology, School of Biomedical Engineering, University of Technology Sydney (UTS), where he leads research on microwave imaging, molecular communications, RF and microwave thermal therapies, implantable and ingestible biomedical devices, array signal processing, wireless biomedical communications, and applied electromagnetics. He is also a Founding Core Member of the Interdisciplinary Research Centre on Health Technologies, UTS. He received a number of competitive research grants from Australian Research Council, National Health and Medical Research Council, and industry. He has also mentored many Ph.D. and master's (research) students. He was a member of the IEEE in New South Wales Section Committee and Technical Program Committee of IEEE GLOBECOM-98 and a past Committee Member of the IEEE NSW Communications and Signal Processing Society chapter. He was a co-recipient of the Priestly Memorial Award from the Institute of Radio and Electronic Engineers, Australia. He was the past Chair of the IEEE NSW AP/MTT joint chapter, the Publicity Co-Chair of the 2011 Asia Pacific Microwave Conference, and the Technical Program Committee Co-Chair of the iWAT2014 and ISAP2015.